The Swift Ultra-Violet/Optical Telescope

Peter W. A. Roming[*a], S. D. Hunsberger[a], Keith O. Mason[b], John A. Nousek[a], Patrick S. Broos[a], Mary J. Carter[b], Barry K. Hancock[b], Howard E. Huckle[b], Tom E. Kennedy[b], Ronnie Killough[c], T. Scott Koch[a], Michael K. McLelland[c], Michael S. Pryzby[d], Phil J. Smith[b], Juan Carlos Soto[e], Joseph Stock[d], Patricia T. Boyd[f], Martin D. Still[g]

[a]Department of Astronomy & Astrophysics, Pennsylvania State University, 525 Davey Lab, University Park, PA 16802, USA

[b]Mullard Space Sciences Laboratory, University College London, Holmbury St. Mary, Dorking, Surrey RH5 6NT, UK

[c]Southwest Research Institute, 6220 Culebra Rd, San Antonio, TX 78228, USA

[d]Swales Aerospace, 5050 Powder Mill Rd, Beltsville, MD 20705, USA

[e]Starsys Research Corporation, 4909 Nautilus Court N., Boulder, CO 80301, USA

[f]University of Maryland, Baltimore County/Laboratory for High Energy Astrophysics, Code 660.1, NASA GSFC, Greenbelt, MD 20771, USA

[g]NASA/Goddard Space Flight Center, Code 660.1, Greenbelt, MD 20771, USA & Universities Space Research Association

ABSTRACT

The UV/optical telescope (UVOT) is one of three instruments flying aboard the Swift Gamma-ray Observatory. It is designed to capture the early (~1 minute) UV and optical photons from the afterglow of gamma-ray bursts as well as long term observations of these afterglows. This is accomplished through the use of UV and optical broadband filters and grisms. The UVOT has a modified Ritchey-Chrétien design with micro-channel plate intensified charged-coupled device detectors that provide sub-arcsecond imaging. Unlike most UV/optical telescopes the UVOT can operate in a photon-counting mode as well as an imaging mode. We discuss some of the science to be pursued by the UVOT and the overall design of the instrument.

Keywords: Swift, UV/Optical Telescope, UVOT, gamma-ray burst, afterglow, spectroscopy, imaging

1. INTRODUCTION

Since the discovery of gamma-ray bursts[1] (GRBs) in 1973, very slow progress has been made in understanding their nature due to their rapid decay in brightness. It was known that the energetics of these explosions were enormous (energies associated with these GRBs are $\sim 10^{54}$ ergs, which is many orders of magnitude higher than supernova explosions[2]). However, many questions remained unanswered. Were GRBs local or cosmological phenomena? What were the astrophysical mechanisms behind these energetic bursts? How could such rapidly fading objects be studied?

[*] Correspondence: Email: roming@astro.psu.edu; Telephone: (814) 865-7750; Fax: (814) 865-6854

In 1997, a hypothesis suggested that x-ray, optical, and radio afterglows should be present after the initial GRB[3], thus allowing time to study these objects. Less than a month later, the first afterglow from GRB 970228 was detected in the x-ray and optical bands[4]. Later, it was confirmed that GRBs are a cosmological phenomena when a redshift of z=0.835 from GRB 970508 was obtained[5]. A couple of years later, the first optical observation of a GRB itself was achieved with the Robotic Optical Transient Search Experiment (ROTSE)[6]. Proposed progenitors of GRBs included neutron star-neutron star and neutron star-black hole mergers[7,8,9] and "failed" supernovae[10] or hypernovae[11]. GRB 990123 was discovered to be offset from the nucleus of the galaxy and therefore provided evidence that the death and/or merger of massive stars was the origin of GRBs[12].

These and other afterglow studies began to unlock the secrets of GRBs. Despite the rapid progress made in understanding GRBs, many questions still remain. What are the progenitors of GRBs? What can GRBs reveal about the early Universe? Are there different classes and sub-classes of bursts? How does the blast wave develop and interact with its environment[13]?

The Swift Medium-class Explorer (MIDEX) mission is a rapidly slewing, multi-wavelength observatory designed to observe GRBs and their afterglows and to answer these questions. The observatory includes three telescopes: the Burst Alert Telescope[14] (BAT), the X-Ray Telescope[15] (XRT), and the Ultra-Violet/Optical Telescope (UVOT). The wavelength coverage provided by these three instruments is 0.2-150 keV and 170-600 nm. An overview of the Swift mission is provided elsewhere[16].

In this paper, we discuss the as-built UVOT and its capabilities, as opposed to a previous paper that described the proposed design[17]. In Sections 2 and 3, we provide a brief overview of the instrument and describe the UVOT and its subsystems. In Sections 4 and 5, we address the UVOT's observing scenarios and the data products that are produced. In Sections 6 and 7, we provide a brief discussion of the instrument calibration and the available data analysis tools. Finally, in Sections 8 and 9, we outline some of the science objectives of the UVOT and provide concluding remarks.

2. OVERVIEW OF UVOT

The UVOT is a modified Ritchey-Chrétien telescope with a 30 cm aperture and an f-number of 12.7 operating in the wavelength range of 170-600 nm. It is mounted on the optical bench (OB) with the BAT and the XRT as shown in Figure 1 and co-aligned with the XRT. An 11-position filter wheel houses UV and optical grisms, a 4x magnifier, broadband UV and optical filters, a clear "white-light" filter, and blocking filter. Photons register on a micro-channel plate intensified charged-coupled device (MIC). These MICs can operate in a photon counting mode and are capable of detecting very low light levels. When flown above the atmosphere the UVOT will possess the equivalent sensitivity of a 4 m ground-based telescope, capable of detecting a 24th magnitude B-star in 1000s using the white-light filter. An outline of the UVOT's characteristics can be found in Table 1.

Telescope	Modified Ritchey-Chrétien
Aperture	30 cm diameter
F-number	12.7
Detector	Intensified CCD
Detector Operation	Photon Counting
Field of View	17 x 17 arcmin^2
Detection Element	256 x 256 pixels
Sampling Element	2048 x 2048 after centroiding
Telescope PSF	0.9 arcsec FWHM @ 350nm
Wavelength Range	170-600 nm
Filters	11
Sensitivity	m_B=24.0 in white light in 1000s
Pixel Scale	0.5 arcsec

Table 1. UVOT Characteristics

The UVOT Telescope Module (TM) boasts a strong heritage from the Optical Monitor (OM) on ESA' s XMM-Newton mission. A discussion of OM is provided elsewhere[18].

Because of the lessons learned from XMM-Newton, problems discovered on OM have been fixed for UVOT. Specifically, the OM yielded ghost images from bright stars outside the field-of-view (FOV), sensitivity reduction (believed to be caused by contamination of optical surfaces), and photon coincidence losses of photons were discovered on OM. Shielding of an invar ring located in the optical train, an enhanced contamination control program as well as the use of UV grade MgF for coating of the mirrors, and coincidence loss correction routines have been incorporated into UVOT.

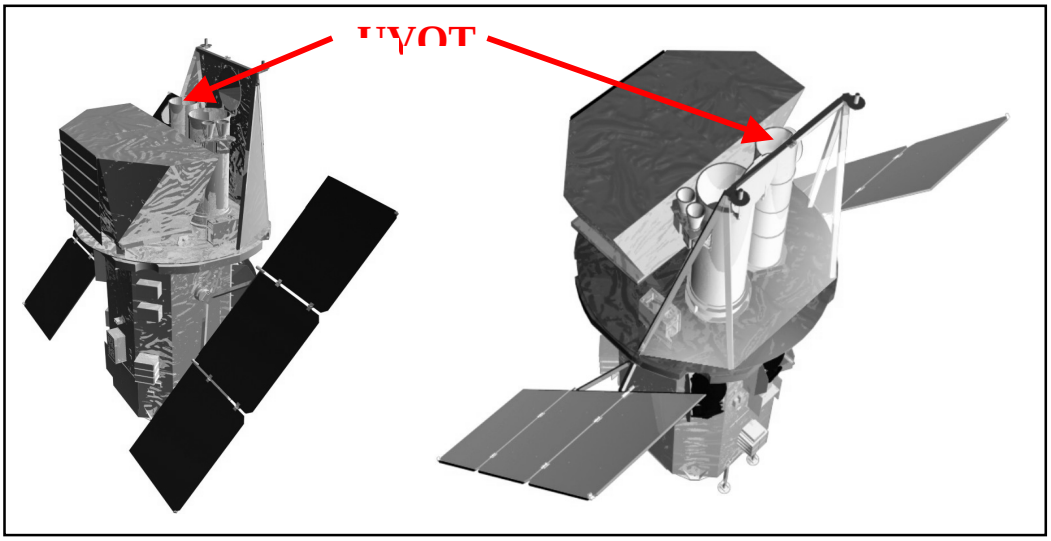

Figure 1. UVOT Placement on the OB

Some of the changes from OM to the UVOT design consist of: new Instrument Control Unit (ICU) software for safing the instrument, a new Digital Processing Unit (DPU), new DPU software to process data, ICU/DPU software to interface with the spacecraft bus, an increase in the allowed number of filter wheel rotations, and a new telescope door based on the Triana[19] door design.

3. UVOT DESCRIPTION

The UVOT consists of 5 units (Figure 2): a TM containing a UV/optical telescope, a Beam Steering Mirror (BSM), two filter wheel mechanisms[1], two photon counting detectors, power supplies, and electronics; two Digital Electronics Modules (DEMs), each one containing a DPU, an ICU, and power supplies for the DPU and ICU; and two Interconnecting Harness Units (IHUs) to connect the TM to the two DEMs. A more detailed sketch of the TM and DEMs can be found in Figures 3 and 4.

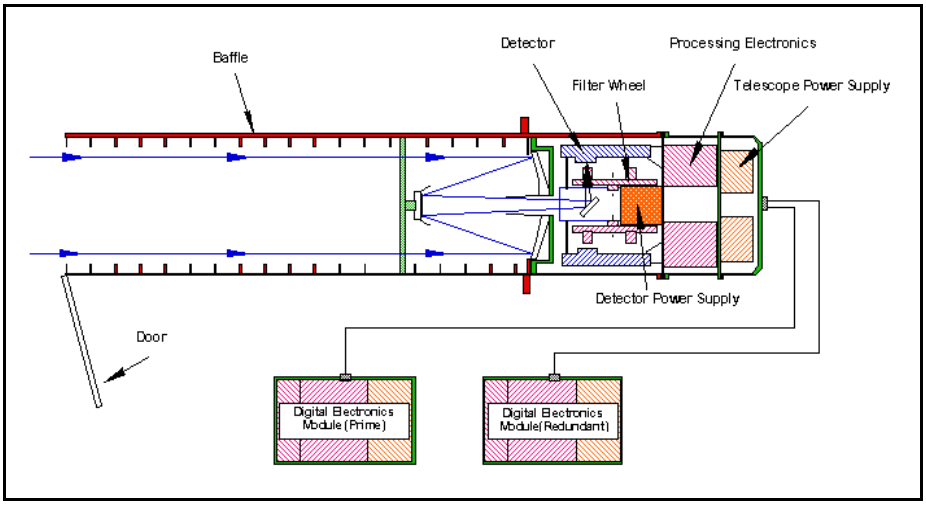

Figure 2. UVOT Schematic

[1] In each case where two units are specified, one unit is a "cold" redundant unit.

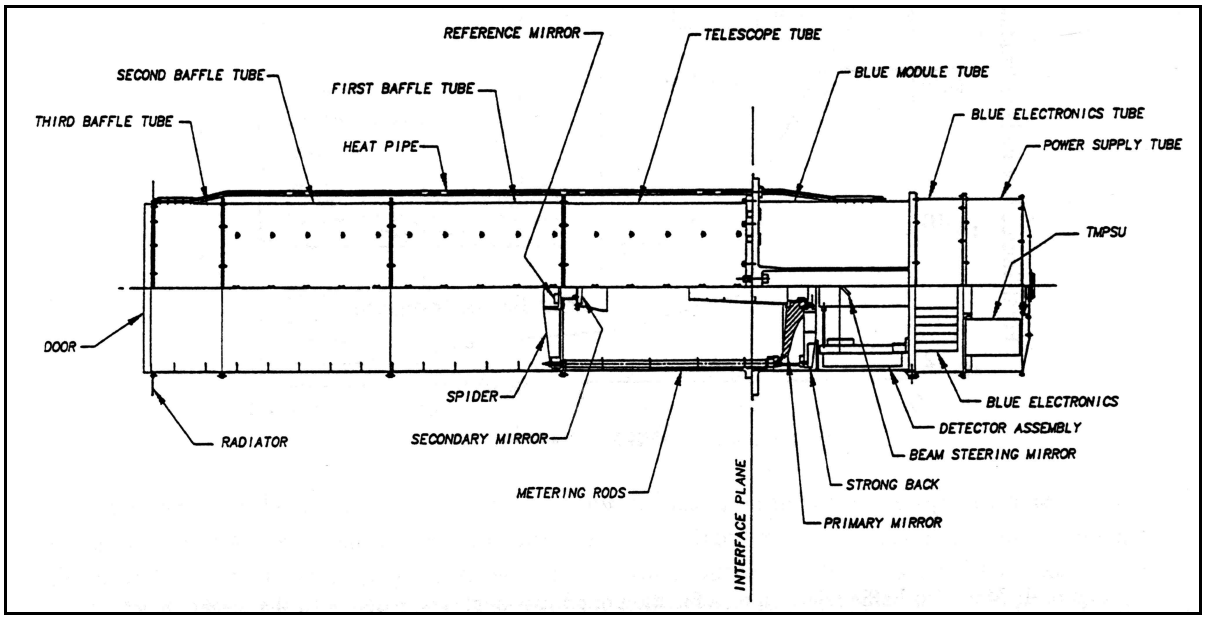

Figure 3. TM Schematic

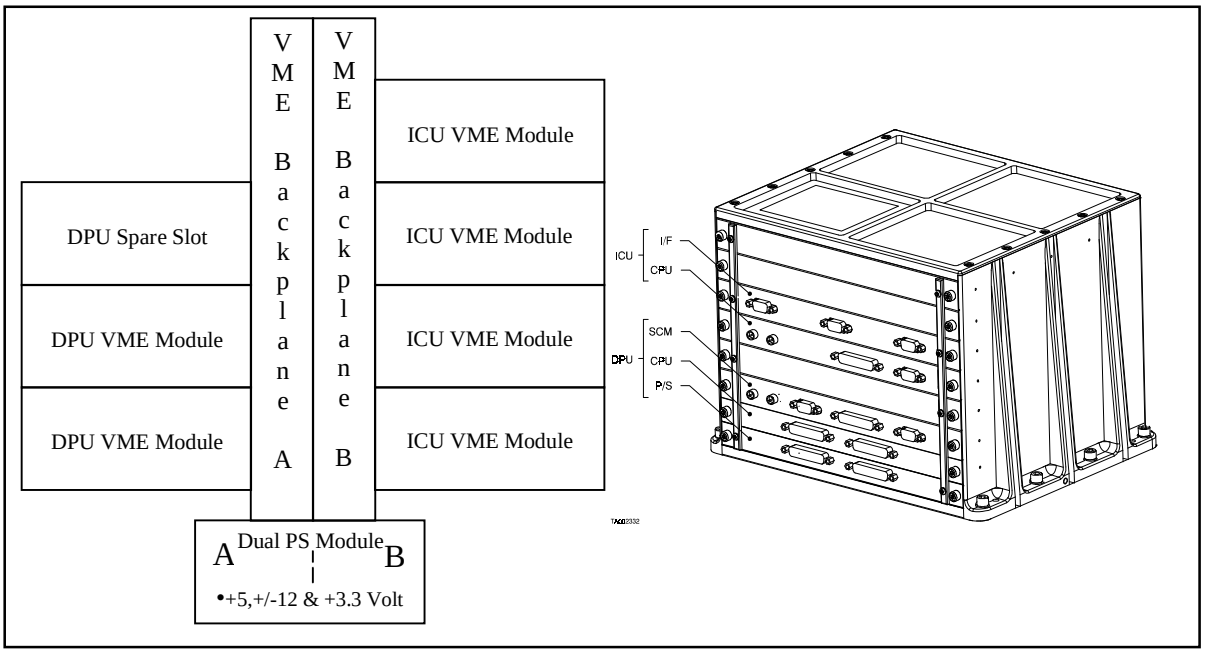

Figure 4. DEM Layout

3.1. Mechanical

The TM is divided into four main sections: external baffle tubes, telescope tube, 'Blue' (or detector) Module Tube (BMT), and TM power supply tube. This subdivision allowed interfaces to be minimized and facilitated the alignment of the optics. The BMT has an external mounting flange that is mounted to the Observatory OB.

The UVOT has four mechanisms: two identical filter wheel mechanisms, the BSM mechanism, and the door module latch mechanism. The filter wheel and beam steering mechanisms are contained in the BMT. The filter wheels rotate on a stub axle which is mounted to base plates (Figure 5). Also attached to the base plates are stepper motors which drive the filter wheels (Figure 6). The BSM mechanism houses a cylinder to which the BSM is attached. The cylinder rotates about the axis of the incident beam by means of the stepper motor. This enables the incident beam to be directed to either the primary or redundant detector assemblies.

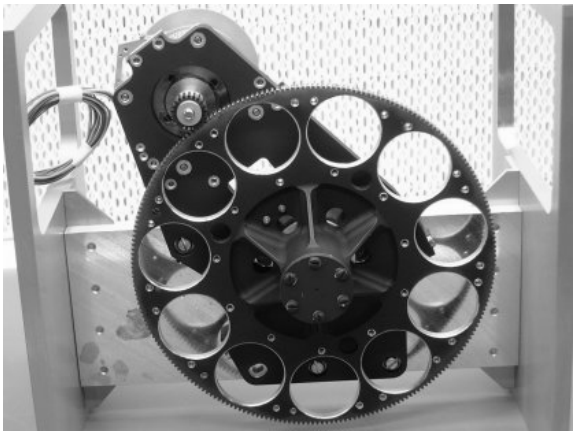

Figure 5. UVOT Filter Wheel Mechanism

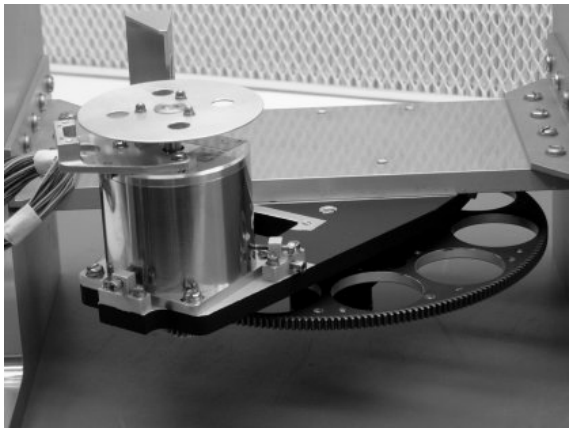

Figure 6. Filter Wheel Stepper Motor

The UVOT door module is designed to minimize contamination within the telescope. The door is held in position by two hinges and a latch. The door module latch mechanism is a mechanically and electrically redundant system with two reacting cup/cones. The latch mechanisms are powered by paraffin driven actuators. When one of the two actuators is powered the shuttle retracts and the latch-plate is released.

At the rear of the BMT and the power supply tube is a bulkhead. The first bulkhead is utilized as the optical bench for the detector assemblies, filter wheels, and the BSM mechanism. The second bulkhead carries the TM Power Supply Unit (TMPSU) which contains the motor drive circuits for the three BMT mechanisms. The two DEMs are mounted separately from the TM onto the OB. Both units are box structures machined from solid magnesium and are designed to minimize cosmic radiation.

3.2. Optics

The telescope tube contains a 30 cm primary and 7.2 cm secondary mirror which are both made from Zerodur. The telescope is a modified Ritchey-Chrétien design. The optical train has a primary f-ratio of f/2.0 increasing to f/12.72 after the secondary. The primary mirror is mounted on a strong back for stability and the secondary mirror is mounted onto spider arms. To maintain focus the mirrors are separated by thermally stable INVAR metering rods (Figure 7). Mounted behind the secondary mirror is a reference mirror that aids in determining UVOT's boresight. The boresight is near the center of the CCDs.

For light rejection there are internal and external baffles. The external baffles consist of the first, second and third baffle tubes, which are forward of the secondary mirrors, and help prevent scattered light from reaching the detectors. The internal baffle lines the inner walls of the telescope tube between the primary and secondary mirrors. Secondary/primary baffles also surround the secondary mirror and the hole at the center of the primary. Behind the primary mirror is the BSM which directs light to one of the two detectors.

Before the light enters the detector it passes through a filter housed in a filter wheel. Each filter wheel contains the following elements: a blocked position for detector safety, UV-grism, UVW2-filter, V-filter, UVM2-filter, optical-grism, UVW1-filter, U-filter, magnifier, B-filter, and White-light-filter. The characteristics of the UVOT lenticular filters can be found in Table 2. The lenticular filter response (Figure 8) and the anticipated grism profiles (Figure 9) are

also provided. The grisms supply a low spectral resolution. The magnifier offers a 4x increase in the image scale which increases the f-ratio to f/54 in the blue and provides diffraction-limited images. It does not operate in the UV because of transmission limitations in this part of the spectrum. Because the focal plane is curved, the filters are weakly figured and the surface of the detector window is concave.

Filter	λ_c (nm)	FWHM (nm)
V	544	75.0
B	439	98.0
U	345	87.5
UVW1	251	70.0
UVM2	217	51.0
UVW2	188	76.0
White	385	260.0

Table 2. UVOT Lenticular Filter Characteristics

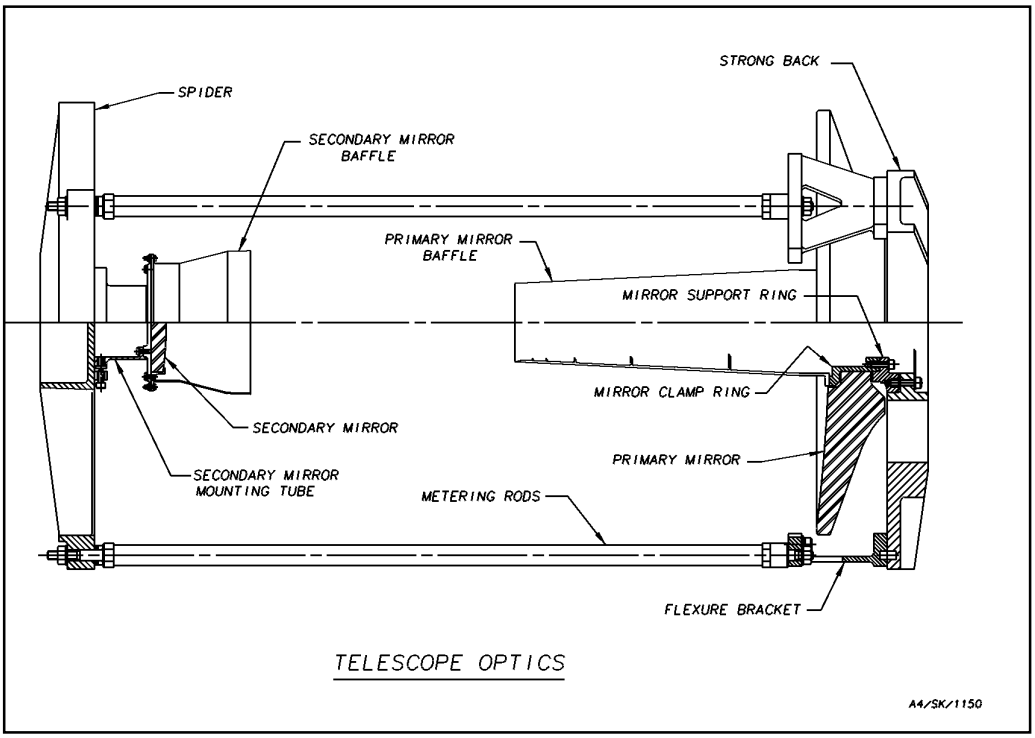

Figure 7. UVOT Telescope Optics

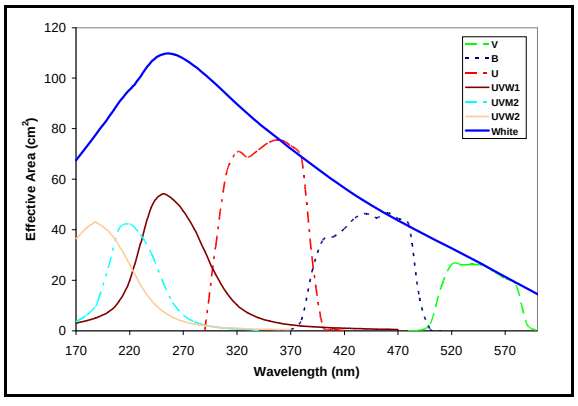

Figure 8. UVOT Lenticular Filter Response

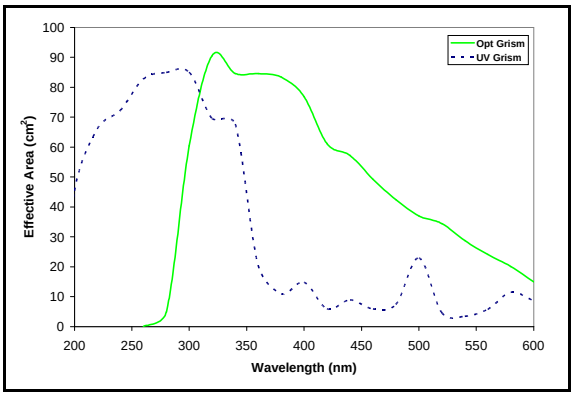

Figure 9. UVOT Anticipated Grism Response

3.3. Detectors

Housed in the BMT are the two detector assemblies. Each detector assembly consists of detector window, a S20 photocathode, three Micro-Channel Plates (MCPs), a phosphor screen, tapered fiber-optics, and a CCD (Figure 10). The CCD has 385 x 288 pixels, 256 x 256 of which are usable for science observations. Each pixel has a size of 4 x 4 arcsec^2 on the sky thus providing a 17 x 17 arcmin^2 FOV. The first MCP has pore sizes of 8 μm with a distance of 10 μm between pore centers. The second and third MCPs have pore sizes of 10 μm with a distance of 12 μm between pore centers. The photocathode is optimized for the UV and blue.

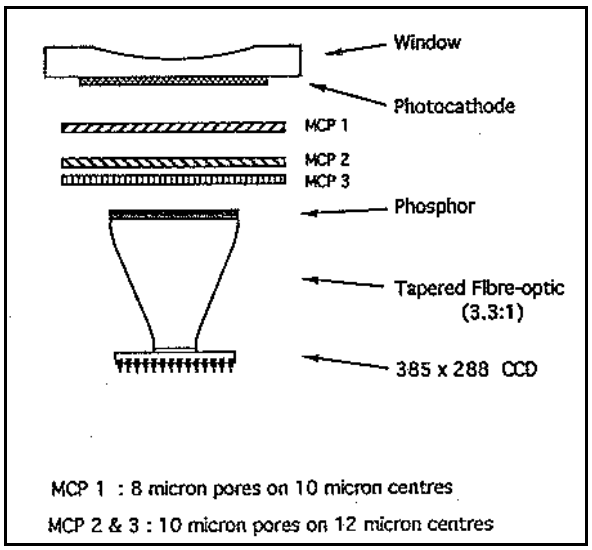

Figure 10. UVOT Detector

Photons arriving from the BSM enter the detector window and hit the photocathode. Electrons emitted from the photocathode are then amplified by the three successive MCPs which in turn illuminate the phosphor screen. The photons from the phosphor screen are then sent through the fiber-optics to the CCD. This affords an amplification of 10^6 of the original signal. The detection of photons is accomplished by reading out the CCD at a high frame rate and determining the photon splash's position using a centroiding algorithm. The detector attains a large format through this centroiding algorithm by sub sampling each of the 256 x 256 CCD pixels into 8 x 8 virtual pixels, thus providing an array of 2048 x 2048 virtual pixels with a size of 0.5 x 0.5 arcsec^2 on the sky. Faint residuals of a pattern formed by creating the 8 x 8 virtual pixels are removed by ground processing. Unlike most UV/optical telescopes, because UVOT's CCD is read out at a high frame rate, the UVOT can be operated in a photon-counting mode.

As with all photon-counting devices there is a maximum count rate threshold. The frame rate of the UVOT detectors is 10.8 ms for a full 17 x 17 arcmin^2 frame; therefore, for count rates above ~10.8 counts/s (for point sources) a dead time correction needs to be applied during the data processing. Details of this dead time correcting can be found elsewhere[20]. In addition, care must be taken when observing bright sources as the local sensitivity of the photocathode is permanently depressed. Autonomous operations diminish the time spent on bright sources (see Section 3.6). The detector's dark noise is extremely low and can be ignored when compared to other sources of background noise.

3.4. Electronics

The UVOT electronics is divided into three basic subsystems: the TM, the prime DEM, and the redundant DEM. The DEMs and TM are interconnected by the interconnecting harnesses. The UVOT redundancy strategy includes cold redundant DEMs and complete electronic redundancy in the TM up to and including the windings of the BSM stepper motor. This requires that the spacecraft supply the UVOT with prime and redundant power as well as Command and Data Handling (C&DH) interfaces.

Most of the electronics for the TM are housed in the BMT. The electronics include the high voltage unit (HVU), the Blue Camera Head (BCH), the Blue Processing Electronics (BPE), and the controls for the filter wheel and BSM. The HVU provides high voltage to the detector system. The unit produces cathode bias voltage, MCP bias voltage, and anode bias voltage. It supplies a voltage safe connector for ground testing and serves as the output monitor for house keeping. The BCH is the CCD readout electronics. It provides pre-amplification of the CCD output, reduction of switching noise, clock sequence generators and drivers, and analogue to digital conversion. The BPE handles the operation of the TM via commands sent from the ICU over the Instrument Control Bus (ICB). The BPE is responsible for producing 11ms CCD frame rates, 10 MHz pixel rates, dynamic dark current subtraction, flood LED control, filter

wheel fine position sensing, thermistor conditioning, centroiding of the 256 x 256 image to a 2048 x 2048 image (as discussed in Section 3.3), and the transfer of the X/Y photon position data to the DPU over the Data Capture Interface (DCI). Additionally, the BPE is tasked with safing the detector from bright sources in the UVOT's FOV. A discussion of this safety circuit can be found elsewhere[21].

The rest of the TM electronics are housed in the rear of the TM in the TM Power Supply Tube (TMPSU). The TMPSU has seven regulated output rails with voltage and current monitoring of secondary rails. It handles input voltages from 24V to 35V. The TMPSU is responsible for the filter wheel and BSM motor drives, and for the filter wheel coarse position monitoring. In addition, the TMPSU handles four primary power heaters which are switched by opto-couplers.

The DEM is the UVOT's high-level command and data processing system. It is comprised of four subsections: the DPU, the ICU, power supply modules, and the Versa Module Eurocard (VME) backplanes (see Figure 4).

The DPU is a two-card assembly: the Central Processing Module containing a RAD 6000 processor and the Swift Communication Module (SCM) which is the card that receives and sends data between the ICU-DPU, BPE-DPU, and the DPU-Spacecraft. The DPU receives a moderate volume of photon data via the DCI and reduces it to a low volume of science telemetry. This science telemetry is then passed to the spacecraft via a 1553 interface. The ICU is also a two-card assembly. It is based on a 31750 16-bit microprocessor. The ICU is the ICB bus master and hosts the software that executes UVOT commands received from the spacecraft; monitors and controls the telescope operations, and generates house keeping telemetry. Communication between the ICU and spacecraft occurs via a 1553 bus and time signals are received using a one-pulse-per-second interface. Communication between the ICU and DPU occurs through the Serial Synchronous Interface (SSI).

The DEM power system includes two independent power supply units. Side A of the DEM furnishes +5V, ±12V, and 3.3V to the DPU and side B distributes +5V to the ICU. The dual power supplies have a nominal input voltage of +32V but accommodate between +22V to +35V. Both power supplies provide electromagnetic and radio frequency interference filtering. The DEM chassis, which includes separate VME backplanes for the DPU and ICU, is based on the SC-9 product[2] made by Southwest Research Institute (SwRI) which was used on the first MIDEX mission - the Imager for Magnetopause-to-Aurora Global Exploration[22] (IMAGE) mission.

3.5. Thermal

The UVOT's thermal design stems from three requirements: during observations, the telescope mounting flange must be maintained at 19.5 ± 0.5 °C to minimize heat transfer between the TM and the OB; the optics portion of the telescope must be maintained at a constant temperature to preserve the separation between the mirrors; and, the operations of the electronics must be protected in order to maintain their proper functions. The thermal control for the TM is active (switched) but passive for the DEMs.

The TM is divided into four thermal zones: telescope tube interior, third baffle tube, telescope tube exterior, and rear exterior of the TM. The telescope tube interior is coated with a high-emissivity black paint while the third baffle tube is coated with a high-emissivity, low-absorptivity white paint. The other external surfaces of the TM are wrapped in Multi-layer Insulation (MLI) in order to limit the heat transfer inside the spacecraft. Figure 11 illustrates the third baffle tube and the telescope tube exterior thermal zones. The telescope door does not have its thermal blanket installed in this configuration.

3.6. Software

An overview of the UVOT software can be found in Figure 12. Both digital electronics units in the UVOT contain microprocessors running custom flight software. The ICU software is responsible for controlling and managing all aspects of the UVOT' s operations, including:

- interacting with the spacecraft bus to ensure instrument safety during slews,

[2] http://www.swri.org/3pubs/ird1999/15909399.htm

- autonomous instrument safing in off-nominal observatory conditions,
- emergency communications via the Tracking and Data Relay Satellite System (TDRSS),
- autonomous protection of the detector from fields containing bright stars,
- interacting with the Figure of Merit[23] computer to select & execute appropriate science observations,
- control and monitoring of instrument thermal state, mechanisms, and detector system.

Many ICU behaviors, most notably the exposure sequences used to observe targets, can be reconfigured via simple table uploads. ICU capabilities are implemented via a combination of compiled Ada code and a custom interpreted scripting language. A detailed description of the ICU software can be found elsewhere[24].

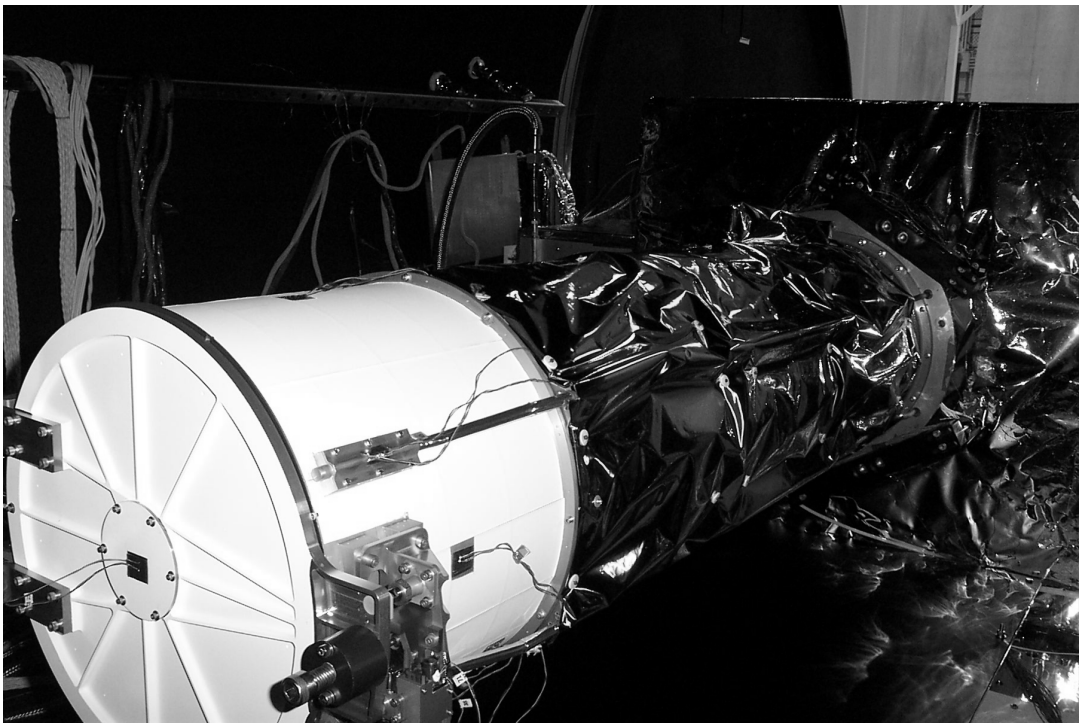

Figure 11. UVOT TM Thermal Design

The DPU software is responsible for reducing and packaging the detector event stream for transport to the ground. Data reduction tasks include spatial windowing of event data (to control telemetry volume), compression of event data, binning of event data into images, compression of images, transformation of engineering data streams into calibration products, and construction of a Finding Chart (which involves source detection; see Sections 4 & 8.2). The DPU contains significant data buffering capacity to accommodate variation in the science data & telemetry production rates.

4. OBSERVING SCENARIOS

There are six observing scenarios for the UVOT: slewing, settling, finding chart, automated targets, pre-planned targets, and safe pointing targets.

Slewing. As the spacecraft slews to a new target, the UVOT does not observe in order to protect itself from bright sources slewing across its FOV and damaging the detector.

Settling. After notification from the spacecraft that the intended object is within ten arcminutes of the target the UVOT begins observing. During this phase pointing errors are off-nominal, i.e., the target is moving rapidly across the FOV as the spacecraft settles. The positional accuracy is only known to a few arcmin based on the BAT's centroided position.

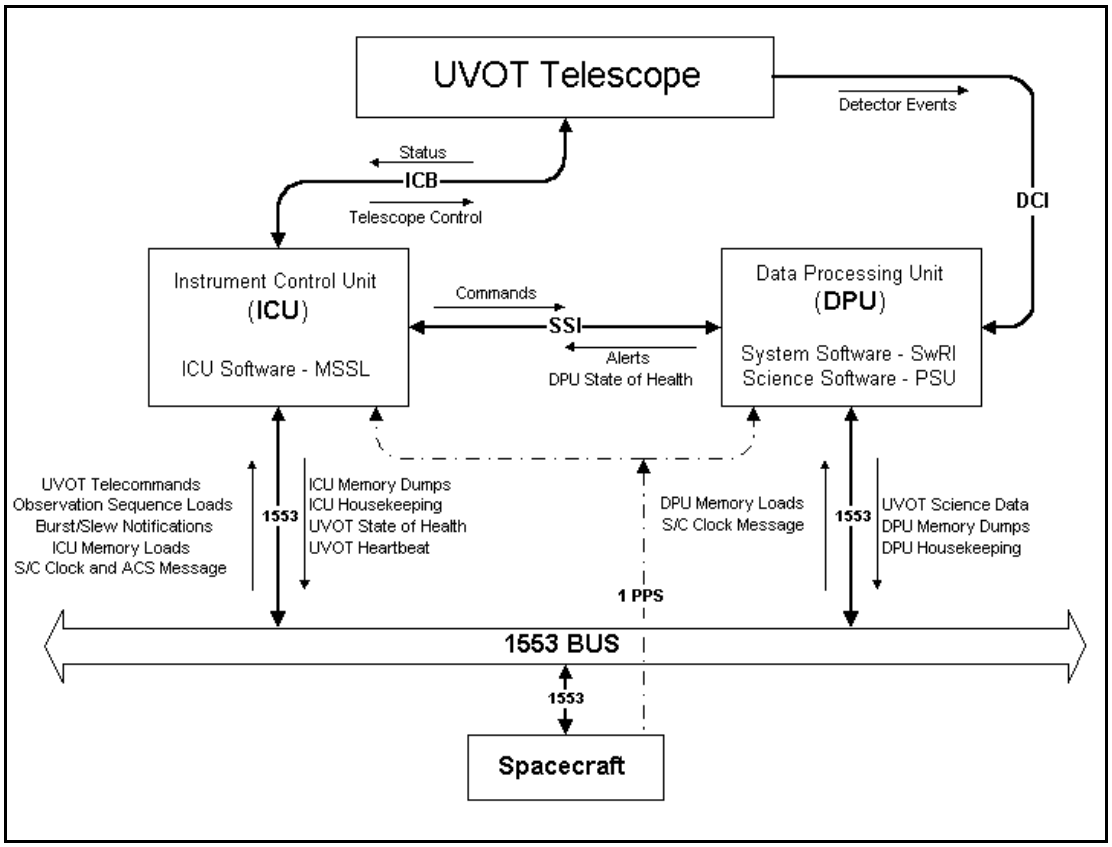

Figure 12. UVOT Software Overview

Finding Chart. If the intended target is a new GRB and the spacecraft is sufficiently settled, i.e., the pointing errors are small, the UVOT begins a 100 second exposure in the V filter to produce a finding chart. The finding chart is to aid ground-based observers in localizing the GRB. The positional accuracy of the finding chart will be approximately 0.3 arcsec relative to the background stars in the FOV. It is anticipated that for most bursts the XRT will have reported a better than 5 arcsec position for the target before the end of the finding chart observation (see Figure 13).

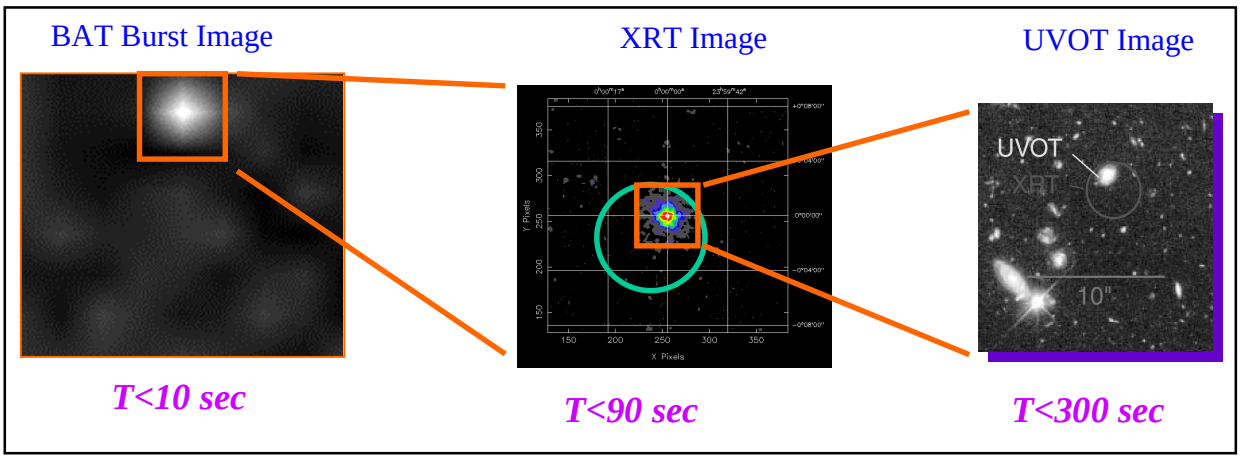

Figure 13. Rapid Position Determination of GRBs

Automated Targets. Once a finding chart has been produced, an automated sequence of exposures, which uses a combination of filters, is executed. The sequence is based on the optical decay profile of the GRB afterglow and time since the initial burst. Currently, two automated sequences will be launched: bright and dim GRB sequences (Figures 14 & 15; BB, UU, W1, GV, M2, VV, W2, & GU in the figures are the B, U, UVW1, Visual Grism, UVM2, V, UVW2, & UV Grism filters respectively; gaps in the figures are due to earth occultation). Although only two sequences will be loaded at launch, new sequences can be added and existing ones modified as GRB afterglows become better understood.

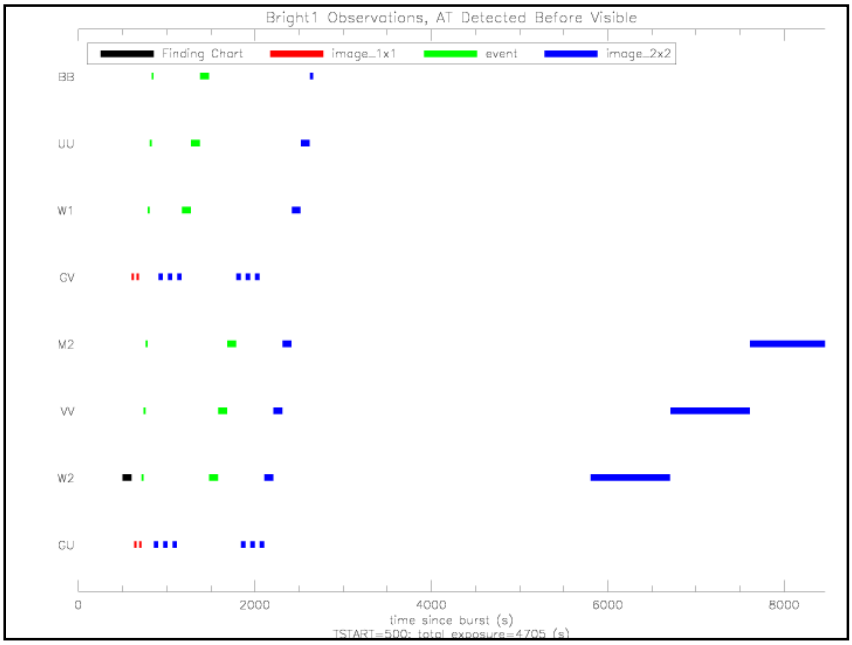

Figure 14. UVOT Bright GRB Sequence (Early GRB Detection)

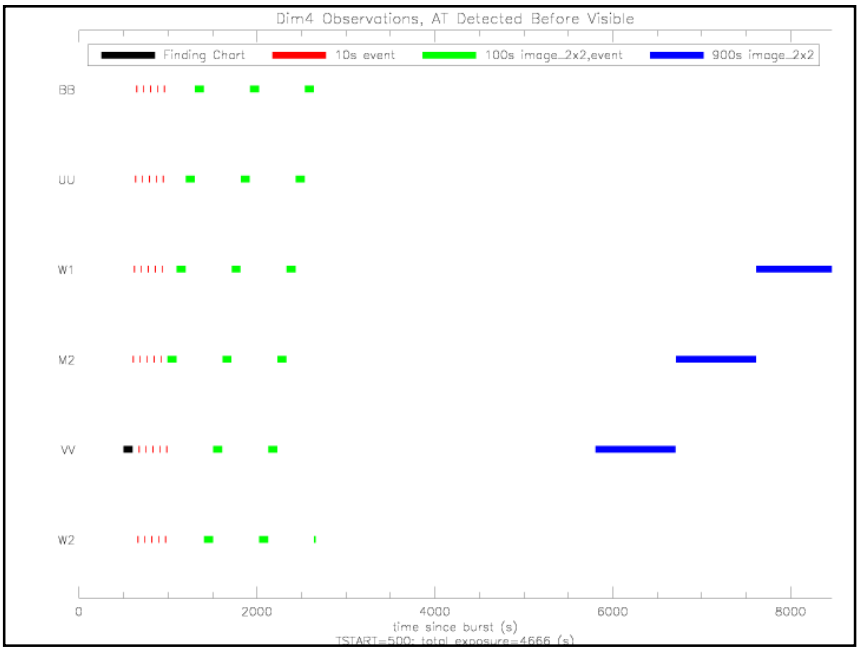

Figure 15. UVOT Dim GRB Sequence (Early GRB Detection)

Pre-Planned Targets. When there are no automated targets, observation of planned targets (which have been uploaded to the spacecraft) begins. Follow-up of previous automated targets, targets-of-opportunity, and survey targets are included as planned targets.

Safe Pointing Targets. When observing constraints do not allow observations of automated or pre-planned targets the spacecraft points to predetermined locations on the sky that are observationally safe for the UVOT.

5. DATA PRODUCTS

The UVOT can produce six types of data products: event lists, images, finding charts, intensifier characteristics, channel boundaries, and centroid confirmation images.

Event List. Each photon event is reported by its position on the detector and the associated CCD frame time-stamp. The accuracy of photon arrival time is dominated by the ambiguity of the CCD frame integration period (11ms).

Image. Image data consist of a 2-D histogram (image) of the event stream, taken over the specified integration period (generally 10-1000s). Image pixels can span 1x1, 2x2, or 4x4 detector sub-pixels. For large numbers of events, image data require much less telemetry than event data, at the expense of greatly reduced time resolution.

Finding Chart. Finding Chart data consist of a small subset of the pixels in an image, carefully chosen to lie under and near the brightest point sources. A "sparse" version of the full image can be constructed on the ground, providing a coarse representation of the detected point sources while consuming modest telemetry volume. Finding chart data are sent immediately via TDRSS, whereas all other science data is stored for later downlinks via a ground station.

Intensifier Characteristics. Intensifier Characteristics data consist of a histogram of the "pulse height" of a set of events obtained with an internal calibration lamp. Examination of these data on the ground assists in adjusting the gains in the detector.

Channel Boundaries. Channel Boundaries data consist of a set of calibration threshold values which, when loaded into the detector electronics, would produce the optimal sub-pixel positioning calculation. The detector data used in the computation of Channel Boundaries are obtained with an internal calibration lamp.

Centroid Confirmation Image. Centroid Confirmation Image data consist of a 2-D histogram which characterizes the bias of the sub-pixel positioning calculation (which is driven by the Channel Boundaries values) across 64 regions of the detector. The detector data used in the computation of a Centroid Confirmation Image are obtained with an internal calibration lamp.

6. CALIBRATION

As part of the UVOT's qualification program, a calibration of the instrument was performed in November, 2002. The following optical procedures were performed on the instrument: point-spread function (PSF) determined, level of in-field scattered light ascertained, global and fine scale non-uniformities characterized, FOV established, distortion characterized, filter throughputs verified, sensitivity limit demonstrated, linearity of detector response characterized, and grism spectral resolution measured. A discussion of the calibration program results and the specialized optical ground support equipment used during the program can be found elsewhere[25,26].

7. DATA ANALYSIS SOFTWARE

The Swift Science Center (SSC) has developed FTOOLs[3,27] for UVOT data analysis which will be available for public download after launch[4]. The tools will operate as stand-alone FTOOLs, within the processing pipeline, or within the user meta-tool "UVOTCHAIN." Once the telemetery has been converted into FITS format, FTOOLs will operate on

[3] See http://heasarc.gsfc.nasa.gov/ftools/
[4] The home page for the SSC can be found at http://swiftsc.gsfc.nasa.gov.

the data. Since the UVOT produces both event and image data products, two sets of tools have been provided. A table of the tools available and a brief description of each tool can be found in Table 3.

Image Data		Event Data	
FTOOL	Description	FTOOL	Description
UVOTBADPIX	Create a 'quality map' of bad pixels	PREFILTER	Generate time-tagged screening parameters
UVOTMODMAP	Reduce pattern noise from virtual pixels		
UVOTFLATFIELD	Correct for pixel sensitivity	COORDINATOR	Coord, distortion & boresight corrections
IMAGEXFORM	Coord, distortion & boresight corrections		
UVOTEXPMAP	Generate exposure map	UVOTSCREEN	Construct GTI tables and screen data
UVOTIMGRISM	Extract grism spectra		
UVOTDETECT	Source detection	UVOTEVGRISM	Extract source events and calculate wavelength
UVOTMAG	Flux calibration		

Table 3. UVOT Data Analysis Tools

8. UVOT SCIENCE GOALS

The top level science goals of the UVOT are to rapidly determine the position of GRBs to sub-arcsecond accuracy, provide spectral or photometric redshifts, identify the GRB environment, and provide timing analysis of GRB afterglows.

8.1 Early Light of GRBs

Because of the rapid slewing capabilities of Swift, the UVOT will be able to capture the early (~30s) UV photons of GRBs during the settling phase (see Section 4), similar to ROTSE's early observations of GRB 990123[28]. All UV photons in the entire 17 x 17 arcmin^2 FOV will be recorded in an event list.

8.2 Rapid GRB Positions

Due to the rapid decline of the afterglow's light-curve, localizing the GRB's position is critical for follow-up observations. The UVOT provides a finding chart as described in Section 4 and 5 above. This finding chart is telemetered to the ground in order to assist ground based observers in pinpointing the burst. This is typically accomplished in less than 300 seconds while the afterglow is still bright.

8.3 Rapid Afterglow Follow-up

After the finding chart exposure has ended, the UVOT begins a several thousand-second automated observation sequence (see Section 4). For bright bursts the filter sequence includes grisms. For fainter targets ($17.0 < m_V < 24.0$), light curves are acquired by cycling through the six broadband filters. Source variability during exposures is monitored by collecting data in event mode.

Swift follow-up of the afterglow is important to our understanding of the GRB environment. Rapid follow-up of GRBs 990123 and 021004 revealed that the afterglow emission was due to reverse external (possibly internal)[29] and superimposed forward-reverse shocks[30], respectively. The UVOT will quickly be able to follow-up many afterglows which will enlarge the current sample significantly. A large database will allow the location and mechanism of the prompt emission to be identified. It will also constrain the Lorentz factor which is a crucial GRB modeling parameter[31]. The image magnifier can be used to determine an accurate position of the GRB within its host galaxy and to detect GRB afterglows to extremely faint magnitudes.

Rapid UVOT follow-up will also facilitate solving the question of "dark" GRBs. Do "dark" bursts have no optical afterglow due to absorption by dust or are their redshifts too high for any optical emission to be present? Are "dark"

bursts simply dim bursts that fade much more quickly than "standard" bursts? Dust absorption by the host galaxy is possible but only if the dust is not destroyed by the burst[32]. GRB 000210 was optically dark. The data suggest that absorption was the probable cause[33]. Evidence that some bursts are dim was verified when GRB 020124 was faintly detected[34]. If GRBs are optically dim, as opposed to dark, then UVOT should be able to follow-up most of these dim afterglows. However, if there is a class of dark bursts, then Swift will quickly provide a XRT arcsec position and a UVOT finding chart for ground based IR telescopes to follow the afterglow.

8.4 Cosmology

Because of the energies involved, GRBs can be used as probes of the early Universe[35]. For bright bursts the UVOT can measure the redshift using the optical and UV grisms. For fainter targets ($17.0 < m_B < 24.0$) photometric redshifts can be obtained in the $1.5 \leq z \leq 3.5$ range.

9. CONCLUSIONS

It is anticipated that the Swift mission will be launched in 2004. The UVOT is an important component to the Swift Observatory. Because of Swift's ability to rapidly slew to a target, the UVOT should be able to capture the early light from some GRBs and will be a dedicated instrument in the follow-up observations of most afterglows. It is anticipated that the UVOT will be key in unraveling such questions as: what are the GRB fireball properties, what are the progenitors of GRBs, are there other class/sub-classes of GRBs, are "dark" bursts due to obscuring dust or are their redshifts too high for optical observations?

ACKNOWLEDGMENTS

We would like to acknowledge the contributions from the many members of the UVOT team. We appreciate the support staff at the following institutions: Penn State University, Mullard Space Science Lab, Southwest Research Institute, Swales Aerospace, NSI, and Goddard Space Flight Center. We would also like to thank John Johnston for his assistance with the electronics section of this paper.

REFERENCES

[1] R. W. Klebesadel, I. B. Strong, & R. A. Olson, "Observations of Gamma-Ray Bursts of Cosmic Origin," *Astrophysical Journal*, **182**, L85-L88, 1973.
[2] P. Mészáros & M. J. Rees, "Tidal Heating and Mass Loss in Neutron Star Binaries: Implications for Gamma-Ray Burst Models," *Astrophysical Journal*, **397**, 570-575, 1992.
[3] P. Mészáros & M. J. Rees, "Optical and Long-Wavelength Afterglow from Gamma-Ray Bursts," *Astrophysical Journal*, **476**, 232-237, 1997.
[4] E. Costa, *et al*, "Discovery of an X-Ray Afterglow Associated with the Gamma-Ray Burst of 28 February 1997," *Nature*, **387**, 783-785, 1997.
[5] M. R. Metzger, S. G. Djorgovski, S. R. Kulkarni, C. C. Steidel, K. L. Adelberger, D. A. Frail, E. Costa, & F. Frontera, "Spectral Constraints on the Redshift of the Optical Counterpart to the γ-Ray Burst of 8 May 1997," *Nature*, **387**, 878-880, 1997.
[6] C. Akerlof, *et al*, "Observations of Contemporaneous Optical Radiation from a γ-Ray Burst," *Nature*, **398**, 400-402, 1999.
[7] J. Goodman, "Are Gamma-Ray Bursts Optically Thick," *Astrophysical Journal*, **308**, L47-L50, 1986.
[8] B. Paczyński, "Gamma-Ray Bursters at Cosmological Distances," *Astrophysical Journal*, **308**, L43-L46, 1986.
[9] R. Narayan, B. Paczyński, & T. Piran, "Gamma-Ray Bursts as the Death Throes of Massive Binary Stars," *Astrophysical Journal*, **395**, L83-L86, 1992.
[10] S. E. Woosley, "Gamma-Ray Bursts from Stellar Mass Accretion Disks Around Black Holes," *Astrophysical Journal*, **405**, 273-277, 1993.
[11] B. Paczyński, "Are Gamma-Ray Bursts in Star-Forming Regions," *Astrophysical Journal*, **494**, L45-L48, 1998.
[12] J. S. Bloom, *et al*, "The Host Galaxy of GRB 990123," *Astrophysical Journal*, **518**, L1-L4, 1999.
[13] N. Gehrels, *et al*, "The Swift Gamma Ray Burst Mission," *Astrophysical Journal*, in prep.

[14] S. D. Barthelmy, "SWIFT Burst Alert Telescope (BAT)," *X-Ray and Gamma-Ray Instrumentation for Astronomy XIII*, *Proc. SPIE* **5165** (these proceedings).
[15] D. N. Burrows, J. E. Hill, & J. A. Nousek, "SWIFT X-Ray Telescope," *X-Ray and Gamma-Ray Instrumentation for Astronomy XIII*, *Proc. SPIE* **5165** (these proceedings).
[16] N. Gehrels, *et al*, "The Swift Gamma Ray Burst Mission," *Astrophysical Journal*, in prep.
[17] P. W. A. Roming, "The Ultra-Violet/Optical Telescope of the Swift MIDEX Mission," *X-Ray and Gamma-Ray Instrumentation for Astronomy XI*, K. A. Flanagan & O. H. W. Siegmund, eds., *Proc. SPIE* **4140**, 76-86, 2000.
[18] K. O. Mason, *et al*, "The XMM-Newton Optical/UV Monitor Telescope," *Astronomy & Astrophysics*, **365**, L36-L44, 2001.
[19] S. A. Gerstl, "Building a Global Hotspot Ecology with Triana Data," *Remote Sensing for Earth Science, Ocean, and Sea Ice Applications*, G. Cecchi, E. T. Engman, & E. Zilioli, eds., *Proc. SPIE* **3868**, 184-194, 1999.
[20] I. I. Antokhin, *et al*, "The Photometric Calibration of the XMM-Newton Optical Monitor," *New Visions of the X-ray Universe in the XMM-Newton and Chandra Era*, F. Jansen, ed., *ESA SP*-488, 2002.
[21] B. K. Hancock & H. Kawakami, "UVOT Bright Source Safing System," *X-Ray and Gamma-Ray Instrumentation for Astronomy XIII*, *Proc. SPIE* **5165** (these proceedings).
[22] W. C. Gibson, *et al*, "The IMAGE Observatory," *Space Science Reviews*, **91**, 15-50, 2000.
[23] J. A. Nousek, "SWIFT GRB Mission," *X-Ray and Gamma-Ray Instrumentation for Astronomy XIII*, *Proc. SPIE* **5165** (these proceedings).
[24] H. E. Huckle & P. J. Smith, "UVOT Autonomous Operations," *X-Ray and Gamma-Ray Instrumentation for Astronomy XIII*, *Proc. SPIE* **5165** (these proceedings).
[25] K. O. Mason, P. Roming, S. Hunsberger, A. Breeveld, T. E. Kennedy, & J. Stock, "Performance of the UV/Optical Telescope (UVOT)," *X-Ray and Gamma-Ray Instrumentation for Astronomy XIII*, *Proc. SPIE* **5165** (these proceedings).
[26] M. A. Quijada, J. Stock, R. Boucarut, T. Madison, & T. Zukowski, "Optical GSE for the Calibration of the Ultraviolet and Optical Telescope (UVOT) for SWIFT," *X-Ray and Gamma-Ray Instrumentation for Astronomy XIII*, *Proc. SPIE* **5165** (these proceedings).
[27] J. K. Blackburn, "FTOOLS: A FITS Data Processing and Analysis Software Package," *Astronomical Data Analysis Software and Systems IV*, R. A. Shaw, H. E. Payne, & J. J. E. Hayes, eds., 1995, *ASP Conf. Ser.* **77**, 367-370.1995.
[28] C. Akerlof, *et al*, "Observations of Contemporaneous Optical Radiation from a γ-Ray Burst," *Nature*, **398**, 400-402, 1999.
[29] P. Mészáros & M. J. Rees, "GRB 990123: Reverse and Internal Shock Flashes and Late Afterglow Behaviour," *Monthly Notices of the Royal Astronomical Society*, **306**, L39-L43, 1999.
[30] S. Kobayashi & B. Zhang, "GRB021004: Reverse Shock Emission," *Astrophysical Journal*, **582**, L75-L78, 2003.
[31] B. Zhang, S. Kobayashi, & P. Mészáros, "Gamma-Ray Burst Early Optical Afterglows: Implications for the Initial Lorentz Factor and the Central Engine," *Astrophysical Journal*, submitted.
[32] D. Lazzati, S. Covino, & G. Ghisellini, "On the Role of Extinction in Failed Gamma-Ray Burst Optical/Infrared Afterglows," *Monthly Notices of the Royal Astronomical Society*, **330**, 583-590, 2002.
[33] L. Piro, *et al*, "The Bright Gamma-Ray Burst of 2000 February 10: A Case Study of an Optically Dark Gamma-Ray Burst," *Astrophysical Journal*, **577**, 680-690, 2002.
[34] E. Berger, *et al*, "The Faint Optical Afterglow and Host Galaxy of GRB 020124: Implications for the Nature of Dark Gamma-Ray Burst," *Astrophysical Journal*, **581**, 981-987, 2002.
[35] D. Q. Lamb, "Highlights of the Rome Workshop on Gamma-Ray Bursts in the Afterglow Era," *Astronomy & Astrophysics Supplement Series*, **138**, 607-615, 1999.